

LLaVA-3D: A Simple yet Effective Pathway to Empowering LMMs with 3D Capabilities

Chenming Zhu^{1,2} Tai Wang^{2,†} Wenwei Zhang² Jiangmiao Pang² Xihui Liu^{1,†}

¹The University of Hong Kong ²Shanghai AI Laboratory

<https://zcmx.github.io/projects/LLaVA-3D>

[†] corresponding author

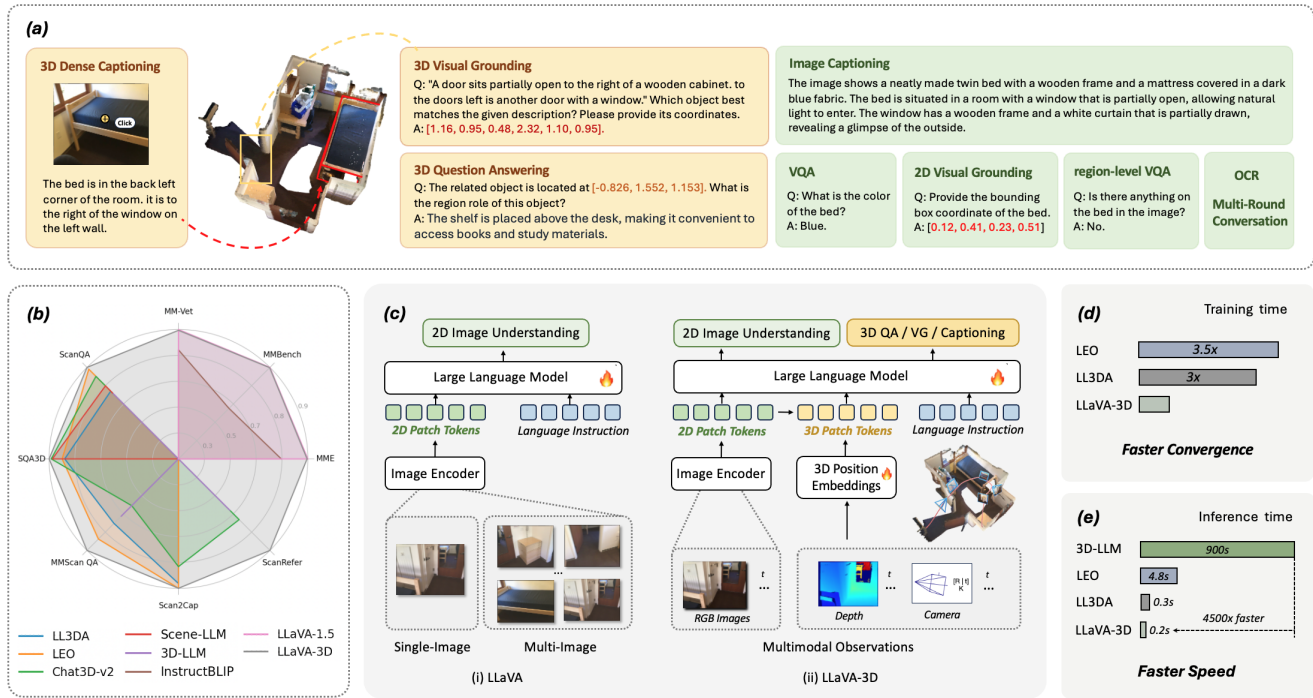


Figure 1. **Overview of LLaVA-3D.** Block (a) shows that LLaVA-3D could perform both 2D and 3D vision-language tasks. The left block (b) shows that compared with previous 3D LMMs, our LLaVA-3D achieves state-of-the-art performance across a wide range of 3D benchmarks while maintaining a comparable performance on various 2D benchmarks compared with LLaVA-1.5. The middle block (c) demonstrates that LLaVA-3D is built on the 2D LLM: LLaVA, and leverages 3D patches to endow it with 3D spatial awareness, enabling it to perform various 3D vision-and-language tasks in the physical world. The right blocks (d) and (e) highlights the significantly faster convergence and inference speeds of LLaVA-3D compared to existing 3D LMMs.

Abstract

Recent advancements in Large Multimodal Models (LMMs) have greatly enhanced their proficiency in 2D visual understanding tasks, enabling them to effectively process and understand images and videos. However, the development of LMMs with 3D scene understanding capabilities has been hindered by the lack of large-scale 3D vision-language datasets and powerful 3D encoders. In this paper, we in-

troduce a simple yet effective framework called **LLaVA-3D**. Leveraging the strong 2D understanding priors from LLaVA, our LLaVA-3D efficiently adapts LLaVA for 3D scene understanding without compromising 2D understanding capabilities. To achieve this, we utilize the 3D position embeddings to bring the 2D CLIP patches within a 3D spatial context. By integrating the 3D position embeddings into 2D LMMs and employing joint 2D and 3D vision-language instruction tuning, we establish a unified architecture for

both 2D image understanding and 3D scene understanding. Experimental results show that LLaVA-3D converges $3.5\times$ faster than existing 3D LMMs when trained on 3D vision-language datasets. Moreover, LLaVA-3D not only achieves state-of-the-art performance across various 3D tasks but also maintains comparable 2D image understanding and vision-language conversation capabilities with LLaVA.

1. Introduction

Recent advancements in Large Multimodal Models (LMMs) [2, 6, 28, 45] have significantly enhanced their ability to understand and reason over visual and language inputs, leading to remarkable performance in 2D visual tasks. Despite their advanced perceptual and reasoning capabilities, LMMs are primarily confined to virtual interactions through images or video, lacking the critical ability to interact with the physical world. To enable their deployment in real-world applications and to facilitate the emergence of new capabilities through physical interactions, it is imperative to equip LMMs with 3D spatial intelligence.

A key aspect of 3D spatial intelligence is the ability to perceive and understand the 3D world. Similar to how 2D LMMs align 2D visual features with language models using large-scale 2D vision-language datasets, a common approach to developing 3D LMMs [9, 17, 18] involves integrating 3D features encoded from point clouds into Large Language Models (LLMs) and training them on 3D point cloud-language datasets. However, in contrast to the abundance of large-scale 2D datasets, 3D datasets remain relatively scarce. Meanwhile, there are no powerful pre-trained 3D point cloud encoders, akin to CLIP ViT [43] in 2D, to provide strong and generalizable 3D features to LLMs.

Since real-world embodied agents typically rely on ego-centric, multi-view images as their raw observations, we aim to build a 3D foundation model based on such inputs rather than 3D point clouds. There have been attempts [15, 16] to leverage the 2D foundation models, like CLIP, alongside LLMs to advance this goal. These methods resort to 2D object segmentation results [24] to extract and aggregate CLIP features from object-centric image patches, constructing pixel-aligned 3D scene features [22]. However, this pipeline is inherently complex and computationally intensive. In contrast, 2D LMMs [2, 6, 28, 35, 36] directly leverage CLIP’s image patch features with richer, fine-grained information for effective image understanding and visual reasoning. This naturally leads to the question: *Can we directly build a 3D LMM upon the strong 2D priors from 2D LMMs, bypassing the obstacles in 3D data scale and 3D encoders?*

In light of recent progress in 2D LMMs, we propose a simple yet effective framework, LLaVA-3D, which extends the well-established 2D LLaVA model to efficiently comprehend the 3D world while preserving its robust 2D

multimodal perception and reasoning capabilities. Inspired by ODIN [21] which leverages the positional encodings for unified 2D and 3D segmentation, our LLaVA-3D encodes the 3D spatial coordinates into 3D position embeddings, and incorporate them into the 2D patches in LLaVA to construct 3D patches. After enhancing the 2D visual tokens with 3D position awareness, we explore various pooling strategies to compress the visual tokens across extensive input frames before being fed into LLM. Fine-tuned on the existing 3D vision-language datasets, our model converges rapidly and acquires 3D spatial understanding and grounding capabilities. Furthermore, the unified model architecture allows LLaVA-3D to retain the strong 2D understanding and reasoning abilities of LLaVA through joint instruction-tuning on 2D vision-language datasets.

Our experimental results demonstrate that LLaVA-3D achieves state-of-the-art performance on a wide range of 3D tasks and benchmarks [3, 5, 11, 40–42, 52], including 3D captioning, 3D question answering, and 3D grounding while requiring significantly less training time and fewer epochs than existing 3D LMMs. Additionally, LLaVA-3D achieves comparable capabilities in 2D image understanding, reasoning, and conversation to LLaVA through joint tuning on 2D and 3D vision-language instructions.

2. Related Work

2D LMMs. Building on the success of recent LLMs, numerous studies [2, 6, 28, 33, 35, 36] explored LMMs that can jointly process visual and linguistic information. For example, LLaVA [35, 36] aligned 2D images with language models through an image encoder and a projection layer, while BLIP2 [28] employed a sophisticated Q-Former architecture to guide the compression of visual features using textual cues. However, most early 2D LMMs were trained on single-image datasets, limiting their ability to tackle multi-image understanding. Recently, there has been increasing interest in expanding LMMs to handle multi-image inputs, addressing the demands of real-world scenarios. For video LMMs [26, 29, 32, 48], multi-image input forms the basis for capturing temporal or action-related dynamics across sequences of video frames. On the other hand, multi-view images of the 3D scene can implicitly reveal 3D spatial relationships and other abstract relations in the environment. Recent works [34, 42] explored whether 2D LMMs [1, 46] can leverage multi-view images to perform spatial understanding. However, these methods primarily relied on implicit learning from the data, without directly modeling the 3D world. In contrast, our LLaVA-3D explicitly models the 3D world from multi-view images, enabling advanced 3D spatial understanding and grounding capabilities.

Injecting 3D into LLMs. As 2D LMMs achieved substantial progress in visual perception, similar efforts have been

made in the 3D domain. For 3D scene-level understanding, recent works explored ways to integrate 3D inputs such as point clouds [9, 17, 18] or multi-view images [15, 16] into LLMs to enable advanced 3D scene understanding and reasoning. An important distinction among these methods is how they construct the 3D scene representation. LL3DA [9] directly used a scene-level 3D point cloud encoder to extract the 3D scene representation. LEO [18] and Chat3D v2 [17] first segmented 3D objects from the scene point cloud using the off-the-shelf 3D instance segmentation model, and then independently extracted 3D object features with object-level 3D encoders to represent the 3D scene. On the other hand, starting from multi-view images, 3D-LLM [16] and Scene-LLM [15] resorted to manually crafted 2D object segmentation to extract and aggregate CLIP features from object-centric image patches, constructing pixel-aligned 3D point representation. Unlike these approaches, our LLaVA-3D directly builds on the well-trained 2D LMM with multi-view images as input. Utilizing the 3D position embeddings, it brings the 2D patches within a 3D spatial context to construct 3D Patches. This 3D representation enables quick adaption of LLaVA for 3D scene understanding while preserving its strong 2D image understanding ability.

Joint Modeling of 2D and 3D. Recent works [21, 37, 38] explored leveraging existing 2D foundation models to enhance 3D perception for detection and segmentation tasks. These methods extract 2D features from multi-view images using 2D foundation models, and then construct 3D position-aware features by incorporating 3D position embeddings for improved 3D detection and segmentation. ODIN [21] utilized the posed RGB-D images as input for 3D instance segmentation. It leverages the powerful 2D pre-trained backbone and differentiates between 2D and 3D features by using distinct learnable position encodings, with 2D features represented by pixel coordinates and 3D features represented by 3D coordinates. This unified architecture facilitated joint training on both 2D and 3D datasets, further enhancing the performance of 3D segmentation. Our LLaVA-3D first integrates the 3D position-aware features into 2D LMMs, enabling 2D LMMs to achieve 3D understanding. Analogous to ODIN [21], this modeling approach enables joint 2D-3D training, allowing the model to process and reason about both 2D and 3D tasks in a unified framework.

3. Method

Previous 2D LMMs typically consist of a visual encoder to extract 2D image features, which are then aligned with the LLM via the projection layer for joint visual and language reasoning tasks. In this section, we introduce how to bridge the 2D image features within 3D spatial context to construct 3D patches (Sec. 3.1, 3.2), and then demonstrate the 3D-aware pooling strategies to compress the 3D patches

(Sec. 3.2) and finally present the 3D-aware position encoding and decoding process (Sec. 3.4), as illustrated in Fig. 2.

3.1. Preliminary

We choose LLaVA [36] as the 2D LMM and explore building a 3D LMM based on it. LLaVA uses the pre-trained CLIP encoder to extract the 2D patch features $X_v \in \mathbb{R}^{c \times w \times h}$ from the image $X \in \mathbb{R}^{3 \times W \times H}$, and then align the 2D patch features X_v into with LLM space with the projection layer. A simple multi-view image adaptation [27] could be extracting multi-view 2D Patch features from multi-view images $X'_v \in \mathbb{R}^{V \times c \times w \times h}$ and sequentially feeding them into LLM for multi-image understanding. To empower LLaVA with 3D awareness, we incorporate the 3D position embeddings into 2D patches to obtain the 3D patches.

3.2. 3D Patch

Our 3D patch representations are built upon the 2D patch features X'_v extracted from multi-view images with CLIP visual encoder to leverage the strong visual-semantic alignment. To construct the 3D patches, we inject the 3D position information into the 2D patches so that the 3D patches can explicitly model 3D spatial information while preserving the semantic information from 2D patches. As illustrated in left block of Fig. 2, given the multi-view 2D patch features $X'_v \in \mathbb{R}^{V \times c \times w \times h}$, we obtain their 3D positions $P \in \mathbb{R}^{V \times 3 \times w \times h}$ in the 3D world, using nearest neighbor depth and known camera intrinsic and extrinsic parameters, following ODIN [21]. The 3D positions P are then encoded into 3D position embeddings $P' \in \mathbb{R}^{V \times w \times h \times d}$ through a learnable two-layer MLP, which are subsequently added to the 2D patch visual tokens, resulting in the 3D patches $X'_{3D} \in \mathbb{R}^{V \times w \times h \times d}$:

$$X'_{3D} = X'_v + P' \quad (1)$$

3.3. 3D Patch Pooling

While 3D patches enhance 2D patches with spatial information, they increase linearly with the number of input images. Since comprehensive 3D scene capture requires numerous images, this creates a substantial computational burden for the LLM. To address this, we introduce a 3D-aware pooling mechanism to reduce the number of 3D patches, as illustrated in the middle block of Fig. 2.

In the 2D image or video domain, pooling is commonly applied along the 2D spatial or temporal dimensions to compress the number of tokens and extract essential semantic information. However, for 3D scene understanding, we must pool the 3D patches based on their 3D locations to ensure these features can cover and preserve the entire scene’s structure as completely as possible. We explore two parameter-free pooling strategies to achieve this:

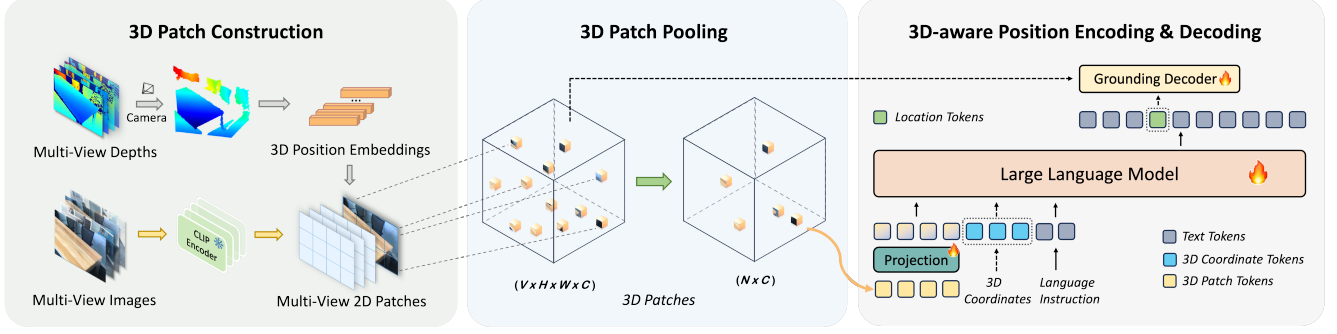


Figure 2. **LLaVA-3D Architecture.** Based on LLaVA, we directly add the corresponding 3D position embeddings to 2D patch visual tokens of multi-view images to construct the 3D Patches, then the 3D Patches will undergo 3D pooling and be sent into the projection layer of LLaVA to map into the LLM space and align with the LLM using 3D-visual-language data.

Voxelization Pooling. Voxelization discretizes the 3D space into a volumetric grid, with 3D patches undergoing average pooling within each occupied voxel, resulting in updated voxel visual tokens. Only the visual tokens from the occupied voxels are passed to the LLM, and the number of tokens varies across different 3D scenes. While the number of 3D patches scales with the number of images, the number of voxel tokens depends solely on the partitioning of the voxel grid. By adjusting the voxel size, we can effectively balance the trade-off between the number of visual tokens and the preservation of fine-grained scene features.

FPS Pooling. Farthest Point Sampling (FPS) is a widely used sampling strategy [20, 39] to select a representative subset of points from a larger set of points cloud. We apply FPS to sample 3D patches from multi-view images to a fixed number of tokens, ensuring that the sampled tokens represent the entire scene structure. While fixing the number of tokens helps the LLM efficiently process visual information, it may also result in loss of scene information.

Compared to FPS Pooling, Voxelization Pooling offers equivalent efficiency in visual token compression while preserving more detailed scene information. Furthermore, the explicit construction of voxel grids can better handle dynamic 3D scene updates, whereas FPS Pooling excels at preserving the overall 3D scene structure. We conduct quantitative experiments in Sec. 5.6 to thoroughly assess the effectiveness of these pooling strategies.

3.4. 3D-aware Position Encoding & Decoding

In the previous sections, we detailed the construction of the 3D scene representation from multi-view images, establishing the foundation for further interaction with the 3D scene. Building on this, the LLM could process multi-modal inputs such as the 3D scene, language instructions, and 3D coordinate cues to generate outputs such as language responses and 3D bounding boxes, as illustrated in the right block of Fig. 2. In this section, we introduce how the model is equipped to

interpret 3D coordinate information from inputs and subsequently output precise 3D bounding boxes when specific location-related task requirements are needed.

Encoding of 3D Coordinate Input. In scenarios such as 3D dense object captioning or object-centric question answering, the language instruction contains 3D coordinates. To handle such tasks, we introduce the *3D Coordinate Token* to allow the model to integrate the provided coordinates as context into its reasoning processes. Specifically, we obtain the 3D coordinate token by feeding the 3D coordinates through a two-layer MLP. These 3D coordinate tokens are fed into LLM together with 3D patch tokens and text tokens, enabling 3D coordinate-aware perception and reasoning.

Decoding of 3D Bounding Box Output. The integration of the 3D coordinate token enables the model to process 3D coordinate information from instructions effectively. However, experiments reveal that directly predicting 3D bounding boxes is non-trivial for the LLM, resulting in notably poor performance in the 3D visual grounding. To handle this, we introduce the *Grounding Decoder*: The process begins with a set of instance queries sampled via Farthest Point Sampling from the 3D scene features. In each decoder layer, these instance queries first cross-attend to the 3D features and then to the embeddings of the location tokens from LLM [52], followed by the self-attention. After each decoder layer, each query will pass through the MLP head to output the 3D bounding box and obtain the corresponding score.

4. Training

To leverage the 2D priors from 2D LMMs, we train our LLaVA-3D model based on the pre-trained LLaVA-1.5. Due to the scarcity of 3D scene-language data, our training procedure comprises two stages for different training targets.

Stage 1: 3D Patch Language Alignment. During the first training stage, we use the region-level and scene-level caption data that describe spatial relationships among 3D ob-

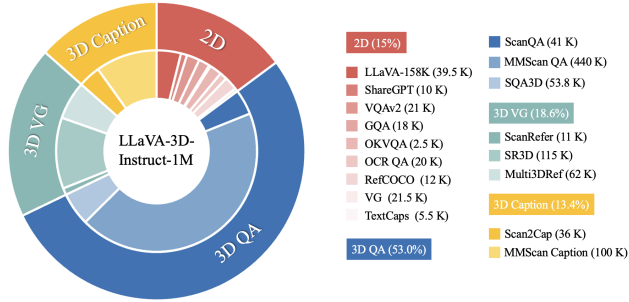


Figure 3. **LLaVA-3D-Instruct-1M**. The hybrid 2D and 3D Dataset Collection. Left: Distribution of data across categories, with the outer circle representing all categories and the inner circle illustrating data subset distribution. Right: Detailed dataset quantities.

jects to align the 3D patches with the LLM for enhanced 3D spatial comprehension. At this stage, the input multi-view images used are selected from sequences that correspond to specific regions or entire scenes. We freeze the vision encoder and LLM and only train the projection layer and 3D position embedding layer for efficient alignment. Since 3D patches are derived from CLIP features augmented with 3D positional information, the alignment between 3D Patch and LLM converges rapidly.

Stage 2: Task Instruction Tuning. During the instruction-tuning stage, LLaVA-3D is optimized to respond to complex 3D V&L tasks and maintain its inherent 2D image reasoning and instruction-following capabilities. To facilitate this capability, we collect the **LLaVA-3D-Instruct-1M** dataset, a hybrid collection of 2D and 3D data specifically tailored for instruction tuning. The overall distribution of the dataset collection is shown in Fig 3, more details about the instructional tuning datasets are listed in the supplementary material. The 2D Data of LLaVA-3D-Instruct-1M is derived from existing LLaVA-1.5 instruction tuning data, ensuring the preservation of 2D image comprehension and conversation abilities. When tuning with 2D data, we keep the vision encoder frozen and jointly train the projection layer and LLM. The 3D Data of LLaVA-3D-Instruct-1M, on the other hand, comprises data from diverse 3D QA, 3D dense captioning, and 3D grounding tasks. During the 3D data instruction tuning, the 3D position embedding layer will be added to jointly train with the other modules. Additionally, for tasks where the instruction contains 3D coordinate information or requires 3D bounding box outputs, the corresponding encoding and decoding modules will be trained together. During instruction tuning, the 3D data pathway includes the 3D position embeddings and 3D patches, while the 2D data pathway is the original LLaVA. All modules except for the 3D position embeddings to construct 3D patches are shared across 2D and 3D data. This training setup ensures that LLaVA-3D is capable of processing both 2D and 3D visual tokens

Table 1. **Quantitative comparison with SOTA models on various 3D QA tasks.** “C” stands for “CIDEr”, “B-4” for “BLEU-4”, “M” for “METEOR”, “R” for “ROUGE”, and “EM@1” for top-1 exact match. Gray indicates evaluation results with refined exact-match protocol.

	ScanQA (val)					SQA3D (test)
	C	B-4	M	R	EM@1	EM@1
Task-specific models						
Scan2Cap [11]	-	-	-	-	-	41.0 [†]
ScanRefer+MCAN [49]	55.4	7.9	11.5	30.0	18.6	-
ClipBERT [25]	-	-	-	-	-	43.3
ScanQA [3]	64.9	10.1	13.1	33.3	21.1	47.2
3D-VisTA [53]	69.6	10.4	13.9	35.7	22.4	48.5
Task-specific fine-tuned 3D LMMs						
3D-LLM (FlanT5) [16]	69.4	12.0	14.5	35.7	20.5	-
LL3DA [35]	76.8	13.5	15.9	37.3	-	-
Chat-3D v2 [17]	87.6	14.0	-	-	-	54.7
LEO [18]	101.4	13.2	20.0	49.2	24.5 (47.6)	50.0 (52.4)
Scene-LLM [15]	80	12.0	16.6	40.0	27.2	54.2
Zero-shot 2D LMMs						
VideoChat2 [30]	49.2	9.6	9.5	28.2	19.2	37.3
LLaVA-NeXT-Video [26]	46.2	9.8	9.1	27.8	18.7	34.2
GPT-4V	59.6	-	13.5	33.4	-	-
Gemini	68.3	-	11.3	35.4	-	-
Claude	57.7	-	10.0	29.3	-	-
LLaVA-3D	91.7	14.5	20.7	50.1	27.0 (45.0)	55.6 (57.6)

effectively, and is adaptive to various task formulations.

5. Experiments

In this section, we conduct extensive evaluations to examine the capabilities of LLaVA-3D. We compare our model’s 3D scene understanding (Sec. 5.1, 5.2, 5.3) and 2D image understanding (Sec. 5.4) capability with previous methods. Then we thoroughly analyze the effectiveness of the components and designs of our LLaVA-3D (Sec. 5.5, 5.6).

5.1. Evaluation on 3D Question Answering

3D Question Answering requires a model to generate responses to the natural language questions in a 3D scene. In this section, we validate LLaVA-3D performance on various 3D question answering benchmarks: ScanQA [3], SQA3D [41], MMScan QA [40], and OpenEQA [42].

Spatial Understanding with ScanQA and SQA3D. ScanQA and SQA3D are both built on the ScanNet dataset. The ScanQA dataset consists of 41363 questions about 800 scenes, including 32337 unique questions. SQA3D comprises 20.4k descriptions of 6.8k unique situations collected from 650 ScanNet scenes and 33.4k questions about these situations. Questions in ScanQA require basic recognition and 3D reasoning capabilities, and SQA3D further incorporates situation understanding and situated reasoning into embodied 3D scene understanding. As shown in Tab. 1, current 2D LMMs fail to achieve competitive performance with the latest 3D LMMs, which might be attributed to the lack of explicit 3D representation. Besides, compared with the 3D LMMs that need to be further fine-tuned on the corresponding datasets, our LLaVA-3D could perform as a generalist

Table 2. **Quantitative comparison on MMScan QA benchmark.** “ST” stands for Single-target, “attr” for attribute, “OO” for Object-Object, and “OR” for Object Region. “S.-BERT”, “B-1”, “B-4”, “R.-L.”, “MET.” represents “Sentence-BERT”, “BLEU-1”, “BLEU-4”, “ROUGE-L”, “METEOR”, respectively. Here, we report the top-1 exact match with (the refined exact-match protocol results) for “EM@1”.

Methods	Setting	Overall	Single-target		Inter-target			Advanced	Data-driven Metrics		Traditional Metrics				
			ST-attr	ST-space	OO-attr	OO-space	OR		SimCSE	S.-BERT	B-1.	B-4.	R.-L	MET.	EM@1
3D-LLM [16]	Zero-Shot	28.6	37.8	18.8	13.7	26.3	15.4	20.8	40.4	40.3	13.4	1.5	17.3	6.0	6.2 (19.6)
Chat3D-v2 [17]		27.9	38.1	18.3	9.3	22.4	13.5	25.4	45.4	46.3	18.0	3.0	22.9	7.5	10.2 (19.6)
LL3DA [9]		15.8	15.5	14.7	14.2	25.2	4.3	6.4	40.7	43.6	5.4	2.1	16.4	4.4	8.3 (19.4)
LEO [18]		22.2	28.9	17.6	18.1	20.4	15.0	16.3	40.4	41.0	11.0	0.7	17.1	4.9	9.6 (18.7)
LL3DA [9]	Fine-tuning	38.5	40.4	46.2	14.7	47.1	26.4	7.1	65.3	67.0	26.4	8.5	44.3	14.7	30.2 (37.6)
LEO [18]		47.8	55.5	49.5	36.1	45.6	32.1	38.4	71.2	72.2	32.0	12.5	52.1	17.7	36.6 (44.5)
LLaVA-3D	Generalist	52.3	61.2	54.4	28.7	61.2	44.5	43.6	74.6	76.3	38.7	13.1	55.5	19.5	45.2 (51.4)

Table 3. **Quantitative comparison with SOTA models on OpenEQA benchmark.**

Models	Frame	Accuracy
LLaMA2 [47]	0	28.3
GPT-4 [1]	0	33.5
Claude3	20	36.3
Gemini-Pro [46]	15	44.9
GPT-4V [1]	15	54.6
GPT-4V [1]	50	55.3
Human	Full	86.8
LLaVA-3D	20	51.2

and achieve the SOTA performance on these benchmarks.

Coordinate Spatial Understanding with MMScan QA.

MMScan QA includes 5.2k scans from ScanNet, 3RScan, and Matterport3D, along with 116k training questions and 29k validation questions. These questions span existential inquiries, attribute understanding, and more advanced queries. Unlike ScanQA and SQA3D, some MMScan QA questions require 3D reasoning based on object coordinates rather than relying solely on text descriptions, demanding the model capable of understanding 3D coordinates information. We present the results under GPT-4 evaluation, data-driven metrics, and traditional metrics respectively in Tab. 2. Our LLaVA-3D achieves significantly better performance compared to LL3DA and LEO which are further fine-tuned on full MMScan QA. The results highlight the training efficiency of LLaVA-3D and its strong 3D understanding ability to serve as the generalist model.

Embodied Question Answering with OpenEQA.

OpenEQA is the first open-vocabulary benchmark designed for spatial understanding and embodied reasoning in embodied question answering. It features an automated evaluation protocol powered by LLMs, which shows strong alignment with human judgment. Our evaluations are conducted using the EM-EQA data split of OpenEQA, which includes over 1,600 high-quality, human-generated questions from diverse real-world environments. The results in Tab. 3 demonstrate that LLaVA-3D surpasses Claude3 and Gemini-Pro, and achieves comparable performance with powerful GPT-4V on this benchmark with significantly

Table 4. **Quantitative Comparisons with SOTA models for 3D Dense Captioning on Scan2Cap.** The n-gram metrics for Scan2Cap are governed by IoU@0.5.

	Scan2Cap (Val)			
	C@0.5↑	B-4@0.5↑	M@0.5↑	R@0.5↑
Scan2Cap [11]	39.1	23.3	22.0	44.8
3D-VLP [23]	55.0	32.3	24.8	51.5
3D-VisTA [53]	61.6	34.1	26.8	55.0
Vote2Cap-DETR [8]	61.8	34.5	26.2	54.4
LL3DA [9]	65.2	36.8	26.0	55.0
LEO [18]	72.4	38.2	27.9	58.1
LLaVA-3D	79.2	41.1	30.2	63.4

Table 5. **Quantitative comparison with SOTA models on the MMScan Captioning benchmark.**

model	Evaluator	Type	Color	Shape	Position	Function	Design	Overall
LL3DA [9]	GPT	10.0	26.3	40.6	38.9	67.5	21.7	33.6
LEO [18]	GPT	34.9	29.7	63.0	63.7	75.0	42.7	51.3
LLaVA-3D	GPT	39.9	79.2	89.1	82.2	94.1	88.0	78.8

fewer model parameters.

5.2. Evaluation on 3D Dense Captioning

3D dense captioning requires the model to localize all the objects in a 3D scene and then generate a descriptive sentence for each object. To evaluate our model on the 3D dense captioning tasks, we utilize the off-the-shelf 3D instance segmentation model [44] to generate object proposals. Then we further construct the 3D coordinate tokens based on the 3D object center coordinates to guide the model in performing the task. Additionally, we utilize two types of textual instructions that prompt the model to either describe the object or describe and output the bounding box of the object. We report the performance of various methods on two 3D dense captioning benchmarks: Scan2Cap and MMScan Captioning.

Scan2Cap. Scan2Cap requires the model to describe the object’s appearance and the spatial relations with nearby objects and output the corresponding 3D bounding box. As illustrated in Tab. 4, our method consistently outperforms the existing method on the Scan2Cap benchmark.

MMScan Captioning. MMScan Captioning focuses on

Table 6. Quantitative comparison with SOTA models on various 3D VG tasks.

	ScanRefer		Multi3DRef	
	Acc@0.25	Acc@0.5	Acc@0.25	Acc@0.5
<i>Task-specific models</i>				
ScanRefer [5]	37.3	24.3	-	-
MVT [19]	40.8	33.3	-	-
3DVG-Trans [51]	45.9	34.5	-	-
ViL3DRel [7]	47.9	37.7	-	-
BUTD-DETR [20]	52.2	39.8	-	-
ReGround3D [52]	53.1	41.1	-	-
M3DRef-CLIP [52]	51.0	44.7	42.8	38.4
<i>Joint-Training 3D LMMs</i>				
3D-LLM [16]	30.3	-	-	-
Chat-3D v2 [17]	35.9	30.4	-	-
Grounded 3D-LLM [10]	47.9	44.1	45.2	40.6
LLaVA-3D	54.1	42.2	54.3	47.2

identifying common aspects of 3D objects such as Object Type, Color, Shape, Position, Function, and Design. The benchmark utilizes GPT-4 to assess whether these aspects are correct in the object description compared with the ground truth description. We benchmark various methods on the MMScan Captioning benchmark in Tab. 5. The results show that our method surpasses existing approaches across all metrics by a substantial margin, especially achieving a 49.5% and 43.3% improvement in the Color score and the Design score respectively. The strong performance further demonstrates the advantages of architectures based on 2D LMMs.

Uniquely, LLaVA-3D takes multi-view images as inputs, enabling a user-friendly feature where users can simply click on the selected images to generate both 3D object captions and 3D bounding boxes. We refer to this capability as *2D Click-based 3D Dense Captioning*, as illustrated in Fig. 4.

5.3. Evaluation on 3D Visual Grounding

3D visual grounding aims to localize the target object in the 3D scene using the natural language description. In this section, we initially report the performance on the ScanRefer [5] and Multi3DRef [50] benchmark. For quantitative comparisons, we include both state-of-the-art task-specific models and joint-training 3D LMMs. 3D-LLM [16] uses the location tokens to discretize the 3D scene and predicts the bounding box as the location tokens that were added to the vocabulary. Chat-3D v2 [17] first segments all the objects and then identify the object that best matches the provided description. The results in Tab. 6 demonstrate that our LLaVA-3D model achieves superior grounding performance compared to methods that rely on heavy 3D instance segmentation as a prerequisite.

5.4. Evaluation on 2D benchmarks

Since our model is trained on the joint 2D and 3D datasets, we evaluate it across various 2D benchmarks to ensure it retains the 2D image understanding capabilities of the original LLaVA. As demonstrated in Tab. 7, LLaVA-3D achieves

Table 7. Quantitative Comparisons on zero-shot 2D benchmarks.

Method	LLM	Res.	VQA ^T	MMB	MME	MM-Vet
MobileVLM [13]	MLLaMA 2.7B	336	47.5	59.6	1289	-
InstructBLIP [14]	Vicuna-7B	224	50.1	36.0	-	26.2
Qwen-VL [4]	Qwen-7B	448	63.8*	38.2	-	-
Qwen-VL-Chat [4]	Qwen-7B	448	61.5*	60.6	1488	-
LLaMA-VID [31]	Vicuna-7B	336	-	65.1	1521	-
LLaVA-1.5 [36]	Vicuna-7B	336	58.2	65.2	1511	31.1
LLaVA-3D	Vicuna-7B	336	57.8	65.0	1502	30.9

Table 8. Architecture Comparison on various 3D V&L Benchmark.

	3D Feature	Connector	LLM / LMM	ScanQA	SQA3D	Inference time
(a)	(SAM + CLIP) w / PE	Q-Former	Vicuna-7B	21.9	49.3	900s
(b)	(SAM + CLIP) w / PE	Pooling + MLP	Vicuna-7B	22.1	49.2	900s
(c)	CLIP w / PE	Pooling + MLP	Vicuna-7B	23.4	51.2	0.2s
(d)	CLIP w / PE	Pooling + MLP	LLaVA-1.5-7B	27.0	55.6	0.2s
(e)	CLIP w / PE	Pooling + MLP	PLLaVA-7B [48]	27.9	56.2	0.2s
(f)	CLIP w / PE	Pooling + MLP	InternVL2-7B [12]	27.6	56.9	0.5s
(g)	CLIP w / PE	Pooling + MLP	InternVL2-20B [12]	28.1	57.1	0.5s

Table 9. Effectiveness of 3D Patch Representation. Training using the same instruction tuning datasets, the only difference between multi-image LLaVA and LLaVA-3D is the patch type.

Method	Patch Type	ScanQA	SQA3D	MMScan QA	Scan2Cap
multi-image LLaVA	2D	24.1	52.3	32.7	29.1
LLaVA-3D	3D	27.0 (+2.9)	55.6 (+3.3)	41.5 (+8.8)	79.2 (+50.1)

performance comparable to LLaVA-1.5 across various 2D image understanding and conversation benchmarks, which the current existing 3D LMMs do not possess. This performance highlights the architectural advantages of our model over other 3D LMMs.

5.5. Architecture Analysis

In this section, we delve deeper into the architectural benefits and efficacy of adapting a 2D large multimodal model (LMM) to a 3D LMM, as opposed to developing a 3D LMM solely from LLMs. A prominent example of the latter approach is 3D-LLM [16], which utilizes established 2D visual foundation models like SAM and CLIP and incorporates 3D multi-view fusion to generate 3D point features, followed by a Q-Former that consolidates these features into a fixed token set.

Architecture Comparison. To ensure the fairness of the experiment as much as possible, starting from LLM, we first ablate different 3D feature encoders, and 3D-language connectors using the same instruction tuning datasets. As shown in Tab. 8, the Q-Former (a) and Pooling + MLP (b) share a similar performance on 3D V&L benchmarks. Notably, using CLIP (c) alone instead of SAM + CLIP (b) achieves better performance and significantly reduces 3D feature extraction computation time from 900s to 0.2s.

Effectiveness of 3D Patch. Once we don’t decorate the 2D patches with corresponding 3D position embedding, LLaVA-

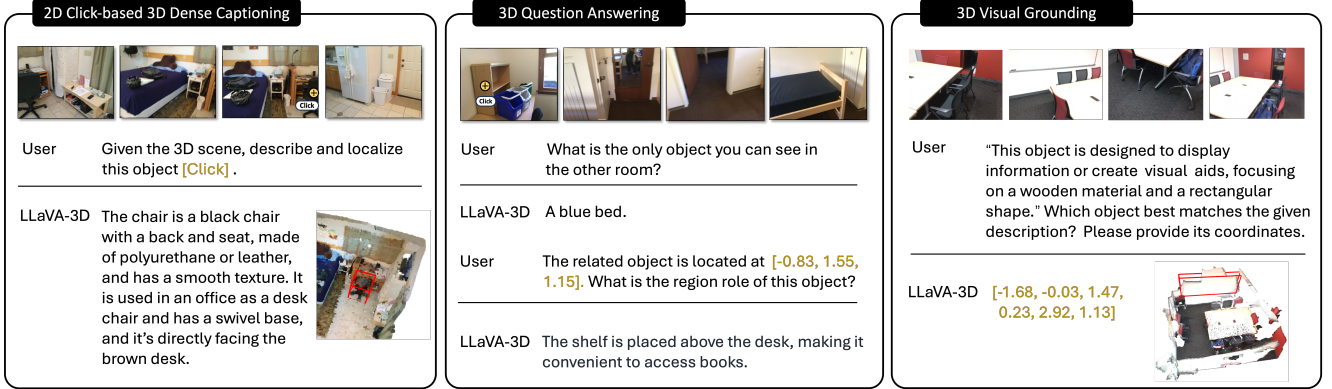


Figure 4. LLaVA-3D enables the user-friendly interaction with the 3D scene across various 3D understanding and reasoning tasks. It allows the users to just click on the 2D images or the video frame to simply conduct the interactive 3D question answering and 3D dense captioning.

3D will degenerate into 2D multi-image LMMs. To further ascertain the efficacy of our proposed 3D Patch, we conduct additional experiments across a variety of 3D question answering and 3D dense captioning benchmarks. As shown in Tab. 9, integrating 2D patches within a 3D context enhances the model’s 3D spatial understanding and reasoning capabilities, resulting in 2.9% and 3.3% improvements on the ScanQA and SQA3D benchmarks, respectively. Furthermore, 3D patches prove instrumental in tasks requiring explicit 3D world modeling, yielding substantial performance gains of 8.8% on the MMScan QA benchmark and a remarkable 50.1% improvement on the Scan2Cap benchmark.

Benefits from pre-trained 2D LMM. Building upon the established 2D LMMs, our framework substantially benefits from comprehensive pre-training and instruction-tuning on extensive image and video-text datasets. In Tab. 8, we explore the advantages of initializing from a pre-trained 2D LMM (d,e,f,g) compared to starting directly from an LLM (c). Our experimental results consistently show that starting with a well-trained 2D LMM significantly improves performance in 3D spatial understanding tasks. Experiment results in (e) show that 2D LMM further trained on the video data could lead to better 3D spatial understanding performance. Besides, the results in (f) and (g) demonstrate that our 3D patch can be applied to various 2D LMMs, and scaling up the model’s parameters further enhances performance. Additionally, we find that initializing from a pre-trained 2D LMM enables LLaVA-3D to achieve a training convergence speed $3.5\times$ faster than that of existing 3D LMMs [9, 18]. Further details are provided in the supplementary.

5.6. More Analysis

To better understand the impact of different components of our LLaVA-3D, we conduct a thorough ablation study on the ScanQA and SQA3D benchmarks.

Impact of Pooling Strategy. Here we conduct various experiments to evaluate the effects of the different pooling

Table 10. Comparison on different pooling strategies.

Pooling Strategy	Voxel Size	Token Number	ScanQA	SQA3D
Voxelization	0.4	Dynamic	24.1	53.2
Voxelization	0.3	Dynamic	25.9	54.8
Voxelization	0.2	Dynamic	27.0	55.6
FPS	-	576	25.7	54.9
FPS	-	1024	26.3	55.2

strategies. For voxelization pooling, we adopt the simple voxelization approach from ODIN [21]. As shown in Tab. 10, the voxelization pooling strategy outperforms the FPS pooling method on 3D QA benchmarks. Model performance can be improved by either decreasing voxel size in voxelization pooling or increasing the number of 3D patch tokens in FPS pooling.

Multi-View Images Sampling Strategy. To balance computational efficiency with visual coverage, we sample V views from the egocentric images of each 3D scene. We investigate two sampling strategies during inference: *Uniform Sampling*, which evenly samples images across the scene, and *Text-Guided Sampling*, which selects frames based on CLIP image-text similarity scores to the input instruction. Since our experiments show a similar performance, we adopt uniform sampling for its simplicity.

Number of Views. An intuitive assumption is that sampling more views from the 3D scene will preserve more information about the 3D scene. We conduct a comparative experiment varying the number of views sampled from 3D scenes. Tab. 11 presents the Exact Match (EM) scores on ScanQA and SQA3D across different settings, revealing that the increase in EM score is marginal as the number of views increases. Additionally, the experimental results indicate that exceeding a certain number of views can degrade the model’s performance.

Table 11. Comparison on performance on 3D QA tasks under different number of multi-view images.

Number of Views	Number of Tokens	ScanQA	SQA3D
16	9216	26.2	55.1
20	11520	27.0	55.6
24	13824	27.0	55.4
40	23040	26.7	55.2

6. Conclusion

We propose LLaVA-3D, a simple yet effective framework built upon the well-established 2D LLaVA model. LLaVA-3D extends the LLaVA’s capabilities to understand the 3D world by using 3D patches to bridge 2D features within a 3D space, enabling spatial understanding while efficiently preserving the original 2D image understanding and reasoning capability. Experimental results show that our method sets new state-of-the-art performance on a wide range of 3D tasks and benchmarks. We hope that our model will inspire new ideas for building 3D LMMs, and in the future, we plan to explore the application of LLaVA-3D in more downstream scenarios, such as robot manipulation and navigation.

References

- [1] Josh Achiam, Steven Adler, Sandhini Agarwal, Lama Ahmad, Ilge Akkaya, Florencia Leoni Aleman, Diogo Almeida, Janko Altmerschmidt, Sam Altman, Shyamal Anadkat, et al. Gpt-4 technical report. *arXiv preprint arXiv:2303.08774*, 2023. 2, 6
- [2] Jean-Baptiste Alayrac, Jeff Donahue, Pauline Luc, Antoine Miech, Iain Barr, Yana Hasson, Karel Lenc, Arthur Mensch, Katherine Millican, Malcolm Reynolds, et al. Flamingo: a visual language model for few-shot learning. *Advances in Neural Information Processing Systems*, 35:23716–23736, 2022. 2
- [3] Daichi Azuma, Taiki Miyanishi, Shuhei Kurita, and Motoaki Kawanabe. Scanqa: 3d question answering for spatial scene understanding. In *proceedings of the IEEE/CVF conference on computer vision and pattern recognition*, pages 19129–19139, 2022. 2, 5
- [4] Jinze Bai, Shuai Bai, Shusheng Yang, Shijie Wang, Sinan Tan, Peng Wang, Junyang Lin, Chang Zhou, and Jingren Zhou. Qwen-vl: A frontier large vision-language model with versatile abilities. *arXiv preprint arXiv:2308.12966*, 2023. 7
- [5] Dave Zhenyu Chen, Angel X Chang, and Matthias Nießner. Scanrefer: 3d object localization in rgb-d scans using natural language. In *European conference on computer vision*, pages 202–221. Springer, 2020. 2, 7
- [6] Jun Chen, Deyao Zhu, Xiaoqian Shen, Xiang Li, Zechun Liu, Pengchuan Zhang, Raghuraman Krishnamoorthi, Vikas Chandra, Yunyang Xiong, and Mohamed Elhoseiny. Minigpt-v2: large language model as a unified interface for vision-language multi-task learning. *arXiv preprint arXiv:2310.09478*, 2023. 2
- [7] Shizhe Chen, Pierre-Louis Guhur, Makarand Tapaswi, Cordelia Schmid, and Ivan Laptev. Language conditioned spatial relation reasoning for 3d object grounding. *Advances in Neural Information Processing Systems*, 35:20522–20535, 2022. 7
- [8] Sijin Chen, Hongyuan Zhu, Xin Chen, Yinjie Lei, Gang Yu, and Tao Chen. End-to-end 3d dense captioning with vote2cap-detr. In *Proceedings of the IEEE/CVF Conference on Computer Vision and Pattern Recognition*, pages 11124–11133, 2023. 6
- [9] Sijin Chen, Xin Chen, Chi Zhang, Mingsheng Li, Gang Yu, Hao Fei, Hongyuan Zhu, Jiayuan Fan, and Tao Chen. Ll3da: Visual interactive instruction tuning for omni-3d understanding reasoning and planning. In *Proceedings of the IEEE/CVF Conference on Computer Vision and Pattern Recognition*, pages 26428–26438, 2024. 2, 3, 6, 8
- [10] Yilun Chen, Shuai Yang, Haifeng Huang, Tai Wang, Ruiyuan Lyu, Runsen Xu, Dahua Lin, and Jiangmiao Pang. Grounded 3d-llm with referent tokens. *arXiv preprint arXiv:2405.10370*, 2024. 7
- [11] Zhenyu Chen, Ali Gholami, Matthias Nießner, and Angel X Chang. Scan2cap: Context-aware dense captioning in rgb-d scans. In *Proceedings of the IEEE/CVF conference on computer vision and pattern recognition*, pages 3193–3203, 2021. 2, 5, 6
- [12] Zhe Chen, Weiyun Wang, Hao Tian, Shenglong Ye, Zhangwei Gao, Erfei Cui, Wenwen Tong, Kongzhi Hu, Jiapeng Luo, Zheng Ma, et al. How far are we to gpt-4v? closing the gap to commercial multimodal models with open-source suites. *arXiv preprint arXiv:2404.16821*, 2024. 7
- [13] Xiangxiang Chu, Limeng Qiao, Xinyang Lin, Shuang Xu, Yang Yang, Yiming Hu, Fei Wei, Xinyu Zhang, Bo Zhang, Xiaolin Wei, et al. Mobilevlm: A fast, reproducible and strong vision language assistant for mobile devices. *arXiv preprint arXiv:2312.16886*, 2023. 7
- [14] Wenliang Dai, Junnan Li, Dongxu Li, Anthony Meng Huat Tiong, Junqi Zhao, Weisheng Wang, Boyang Li, Pascale Fung, and Steven Hoi. Instructblip: Towards general-purpose vision-language models with instruction tuning, 2023. 7
- [15] Rao Fu, Jingyu Liu, Xilun Chen, Yixin Nie, and Wenhan Xiong. Scene-llm: Extending language model for 3d visual understanding and reasoning. *arXiv preprint arXiv:2403.11401*, 2024. 2, 3, 5
- [16] Yining Hong, Haoyu Zhen, Peihao Chen, Shuhong Zheng, Yilun Du, Zhenfang Chen, and Chuang Gan. 3d-llm: Injecting the 3d world into large language models. *arXiv preprint arXiv:2307.12981*, 2023. 2, 3, 5, 6, 7
- [17] Haifeng Huang, Zehan Wang, Rongjie Huang, Luping Liu, Xize Cheng, Yang Zhao, Tao Jin, and Zhou Zhao. Chat-3d v2: Bridging 3d scene and large language models with object identifiers. *arXiv preprint arXiv:2312.08168*, 2023. 2, 3, 5, 6, 7
- [18] Jiangyong Huang, Silong Yong, Xiaoqian Ma, Xiongkun Linghu, Puhao Li, Yan Wang, Qing Li, Song-Chun Zhu, Baoxiong Jia, and Siyuan Huang. An embodied generalist agent in 3d world. *arXiv preprint arXiv:2311.12871*, 2023. 2, 3, 5, 6, 8
- [19] Shijia Huang, Yilun Chen, Jiaya Jia, and Liwei Wang. Multi-view transformer for 3d visual grounding. In *Proceedings of*

- the *IEEE/CVF Conference on Computer Vision and Pattern Recognition*, pages 15524–15533, 2022. 7
- [20] Ayush Jain, Nikolaos Gkanatsios, Ishita Mediratta, and Katerina Fragkiadaki. Bottom up top down detection transformers for language grounding in images and point clouds. In *Computer Vision—ECCV 2022: 17th European Conference, Tel Aviv, Israel, October 23–27, 2022, Proceedings, Part XXXVI*, pages 417–433. Springer, 2022. 4, 7
- [21] Ayush Jain, Pushkal Katara, Nikolaos Gkanatsios, Adam W Harley, Gabriel Sarch, Kriti Aggarwal, Vishrav Chaudhary, and Katerina Fragkiadaki. Odin: A single model for 2d and 3d segmentation. In *Proceedings of the IEEE/CVF Conference on Computer Vision and Pattern Recognition*, pages 3564–3574, 2024. 2, 3, 8
- [22] Krishna Murthy Jatavallabhula, Alihusein Kuwajerwala, Qiao Gu, Mohd Omama, Tao Chen, Shuang Li, Ganesh Iyer, Soroush Saryazdi, Nikhil Keetha, Ayush Tewari, et al. Conceptfusion: Open-set multimodal 3d mapping. *arXiv preprint arXiv:2302.07241*, 2023. 2
- [23] Zhao Jin, Munawar Hayat, Yuwei Yang, Yulan Guo, and Yinye Lei. Context-aware alignment and mutual masking for 3d-language pre-training. In *Proceedings of the IEEE/CVF Conference on Computer Vision and Pattern Recognition*, pages 10984–10994, 2023. 6
- [24] Alexander Kirillov, Eric Mintun, Nikhila Ravi, Hanzi Mao, Chloe Rolland, Laura Gustafson, Tete Xiao, Spencer Whitehead, Alexander C Berg, Wan-Yen Lo, et al. Segment anything. In *Proceedings of the IEEE/CVF International Conference on Computer Vision*, pages 4015–4026, 2023. 2
- [25] Jie Lei, Linjie Li, Luwei Zhou, Zhe Gan, Tamara L Berg, Mohit Bansal, and Jingjing Liu. Less is more: Clipbert for video-and-language learning via sparse sampling. In *Proceedings of the IEEE/CVF conference on computer vision and pattern recognition*, pages 7331–7341, 2021. 5
- [26] Bo Li, Yuanhan Zhang, Dong Guo, Renrui Zhang, Feng Li, Hao Zhang, Kaichen Zhang, Yanwei Li, Ziwei Liu, and Chunyuan Li. Llava-onevision: Easy visual task transfer. *arXiv preprint arXiv:2408.03326*, 2024. 2, 5
- [27] Feng Li, Renrui Zhang, Hao Zhang, Yuanhan Zhang, Bo Li, Wei Li, Zejun Ma, and Chunyuan Li. Llava-next-interleave: Tackling multi-image, video, and 3d in large multimodal models. *arXiv preprint arXiv:2407.07895*, 2024. 3
- [28] Junnan Li, Dongxu Li, Silvio Savarese, and Steven Hoi. Blip-2: Bootstrapping language-image pre-training with frozen image encoders and large language models. *arXiv preprint arXiv:2301.12597*, 2023. 2
- [29] KunChang Li, Yanan He, Yi Wang, Yizhuo Li, Wenhai Wang, Ping Luo, Yali Wang, Limin Wang, and Yu Qiao. Videochat: Chat-centric video understanding. *arXiv preprint arXiv:2305.06355*, 2023. 2
- [30] Kunchang Li, Yali Wang, Yanan He, Yizhuo Li, Yi Wang, Yi Liu, Zun Wang, Jilan Xu, Guo Chen, Ping Luo, et al. Mvbench: A comprehensive multi-modal video understanding benchmark. In *Proceedings of the IEEE/CVF Conference on Computer Vision and Pattern Recognition*, pages 22195–22206, 2024. 5
- [31] Yanwei Li, Chengyao Wang, and Jiaya Jia. Llama-vid: An image is worth 2 tokens in large language models. *arXiv preprint arXiv:2311.17043*, 2023. 7
- [32] Bin Lin, Bin Zhu, Yang Ye, Munan Ning, Peng Jin, and Li Yuan. Video-llava: Learning united visual representation by alignment before projection. *arXiv preprint arXiv:2311.10122*, 2023. 2
- [33] Ji Lin, Hongxu Yin, Wei Ping, Pavlo Molchanov, Mohammad Shoeybi, and Song Han. Vila: On pre-training for visual language models. In *Proceedings of the IEEE/CVF Conference on Computer Vision and Pattern Recognition*, pages 26689–26699, 2024. 2
- [34] Benlin Liu, Yuhao Dong, Yiqin Wang, Yongming Rao, Yansong Tang, Wei-Chiu Ma, and Ranjay Krishna. Coarse correspondence elicit 3d spacetime understanding in multimodal language model. *arXiv preprint arXiv:2408.00754*, 2024. 2
- [35] Haotian Liu, Chunyuan Li, Qingyang Wu, and Yong Jae Lee. Visual instruction tuning. *arXiv preprint arXiv:2304.08485*, 2023. 2, 5
- [36] Haotian Liu, Chunyuan Li, Yuheng Li, and Yong Jae Lee. Improved baselines with visual instruction tuning. In *Proceedings of the IEEE/CVF Conference on Computer Vision and Pattern Recognition*, pages 26296–26306, 2024. 2, 3, 7
- [37] Yingfei Liu, Tiancai Wang, Xiangyu Zhang, and Jian Sun. Petr: Position embedding transformation for multi-view 3d object detection. In *European Conference on Computer Vision*, pages 531–548. Springer, 2022. 3
- [38] Yingfei Liu, Junjie Yan, Fan Jia, Shuailin Li, Aqi Gao, Tiancai Wang, and Xiangyu Zhang. Petr2: A unified framework for 3d perception from multi-camera images. In *Proceedings of the IEEE/CVF International Conference on Computer Vision*, pages 3262–3272, 2023. 3
- [39] Ze Liu, Zheng Zhang, Yue Cao, Han Hu, and Xin Tong. Group-free 3d object detection via transformers. In *Proceedings of the IEEE/CVF International Conference on Computer Vision*, pages 2949–2958, 2021. 4
- [40] Ruiyuan Lyu, Tai Wang, Jingli Lin, Shuai Yang, Xiaohan Mao, Yilun Chen, Runsen Xu, Haifeng Huang, Chenming Zhu, Dahua Lin, et al. Mmscan: A multi-modal 3d scene dataset with hierarchical grounded language annotations. *arXiv preprint arXiv:2406.09401*, 2024. 2, 5
- [41] Xiaojian Ma, Silong Yong, Zilong Zheng, Qing Li, Yitao Liang, Song-Chun Zhu, and Siyuan Huang. Sqa3d: Situated question answering in 3d scenes. *arXiv preprint arXiv:2210.07474*, 2022. 5
- [42] Arjun Majumdar, Anurag Ajay, Xiaohan Zhang, Pranav Putta, Sriram Yenamandra, Mikael Henaff, Sneha Silwal, Paul Mcvay, Oleksandr Maksymets, Sergio Arnaud, et al. Openeqa: Embodied question answering in the era of foundation models. In *Proceedings of the IEEE/CVF Conference on Computer Vision and Pattern Recognition*, pages 16488–16498, 2024. 2, 5
- [43] Alec Radford, Jong Wook Kim, Chris Hallacy, Aditya Ramesh, Gabriel Goh, Sandhini Agarwal, Girish Sastry, Amanda Askell, Pamela Mishkin, Jack Clark, et al. Learning transferable visual models from natural language supervision. In *International conference on machine learning*, pages 8748–8763. PMLR, 2021. 2

- [44] Jonas Schult, Francis Engelmann, Alexander Hermans, Or Litany, Siyu Tang, and Bastian Leibe. Mask3d: Mask transformer for 3d semantic instance segmentation. In *2023 IEEE International Conference on Robotics and Automation (ICRA)*, pages 8216–8223. IEEE, 2023. 6
- [45] Mohit Shridhar, Lucas Manuelli, and Dieter Fox. Perceiver-actor: A multi-task transformer for robotic manipulation. In *Conference on Robot Learning*, pages 785–799. PMLR, 2023. 2
- [46] Gemini Team, Rohan Anil, Sebastian Borgeaud, Yonghui Wu, Jean-Baptiste Alayrac, Jiahui Yu, Radu Soricut, Johan Schalkwyk, Andrew M Dai, Anja Hauth, et al. Gemini: a family of highly capable multimodal models. *arXiv preprint arXiv:2312.11805*, 2023. 2, 6
- [47] Hugo Touvron, Louis Martin, Kevin Stone, Peter Albert, Amjad Almahairi, Yasmine Babaei, Nikolay Bashlykov, Soumya Batra, Prajjwal Bhargava, Shruti Bhosale, et al. Llama 2: Open foundation and fine-tuned chat models. *arXiv preprint arXiv:2307.09288*, 2023. 6
- [48] Lin Xu, Yilin Zhao, Daquan Zhou, Zhijie Lin, See Kiong Ng, and Jiashi Feng. Pllava: Parameter-free llava extension from images to videos for video dense captioning. *arXiv preprint arXiv:2404.16994*, 2024. 2, 7
- [49] Zhou Yu, Jun Yu, Yuhao Cui, Dacheng Tao, and Qi Tian. Deep modular co-attention networks for visual question answering. In *Proceedings of the IEEE/CVF conference on computer vision and pattern recognition*, pages 6281–6290, 2019. 5
- [50] Yiming Zhang, ZeMing Gong, and Angel X Chang. Multi3drefer: Grounding text description to multiple 3d objects. In *Proceedings of the IEEE/CVF International Conference on Computer Vision*, pages 15225–15236, 2023. 7
- [51] Lichen Zhao, Daigang Cai, Lu Sheng, and Dong Xu. 3dvg-transformer: Relation modeling for visual grounding on point clouds. In *Proceedings of the IEEE/CVF International Conference on Computer Vision*, pages 2928–2937, 2021. 7
- [52] Chenming Zhu, Tai Wang, Wenwei Zhang, Kai Chen, and Xihui Liu. Empowering 3d visual grounding with reasoning capabilities. *arXiv preprint arXiv:2407.01525*, 2024. 2, 4, 7
- [53] Ziyu Zhu, Xiaojian Ma, Yixin Chen, Zhidong Deng, Siyuan Huang, and Qing Li. 3d-vista: Pre-trained transformer for 3d vision and text alignment. *arXiv preprint arXiv:2308.04352*, 2023. 5, 6